Received: 16 March 2017 | Revised: 1 December 2017 | Accepted: 10 January 2018

DOI: 10.1002/joc.5450

International Journal of Climatology RMetS

RESEARCH ARTICLE

Integrated kinetic energy of Atlantic tropical cyclones in a global ocean surface wind analysis

Sean Buchanan[1,2,3] | Vasubandhu Misra[1,2,3] | Amit Bhardwaj[2,3]

[1]Department of Earth, Ocean and Atmospheric Science, Florida State University, Tallahassee, Florida

[2]Center for Ocean-Atmospheric Prediction Studies, Florida State University, Tallahassee, Florida

[3]Florida Climate Institute, Florida State University, Tallahassee, Florida

Correspondence
V. Misra, Department of Earth, Ocean and Atmospheric Science, Florida State University, Tallahassee, FL.
Email: vmisra@fsu.edu

Funding information
Climate Program Office, Grant/Award number: NA12OAR4310078; U.S. Geological Survey, Grant/Award number: G13AC00408; FSU IDEA

The integrated kinetic energy (IKE) of a tropical cyclone (TC), a volume integration of the surface winds around the centre of the TC, is computed from a comprehensive surface wind (National Aeronautics and Space Administration's (NASA) cross-calibrated multi-platform [CCMP]) analysis available over the global oceans to verify against IKE from wind radii estimates of extended best-track data maintained by NOAA for the North Atlantic TCs. It is shown that CCMP surface wind analysis severely underestimates IKE largely from not resolving hurricane force winds for majority of the Atlantic TCs, under sampling short-lived and small-sized TCs. The seasonal cycle of the North Atlantic TC IKE also verifies poorly in the CCMP analysis. In this article we introduce proxy IKE (PIKE) based on the kinetic energy of the winds at the radius of the last closed isobar (ROCI), which shows promise for a wide range of TC sizes including the smaller-sized TCs unresolved in the CCMP data set.

KEYWORDS
integrated kinetic energy, reanalysis, tropical cyclones

1 | INTRODUCTION

Atmospheric and oceanographic reanalysis are major accomplishments achieved by the scientific community that have opened doors of understanding the complexities of climate and its variations over the years. In particular, tropical cyclone (TC) studies have utilized such advancements to understand their structure, dynamics and influence on climate variability. For instance, Hart, Maue, and Watson (2007) studied the local memory of atmospheric and oceanic variability after TC passage using the 40-year European Centre for Medium-Range Weather Forecasts (ECMWF) Re-Analysis (ERA-40); Sriver and Huber (2007) examined the average oceanic heat transport by TCs; Hart (2011) examined the influence of TC activity on polewards heat transport through changes to the meridional heat flux. However, the constant concern of coarse grid resolution, limitations of the physics and dynamics of the data assimilation models, the shortcomings of data assimilation methodologies, observational errors and scarcity of observations representing TCs in the reanalysis have always persisted. For example, the limitations of atmospheric reanalysis in representing the intensity and location of the TCs are highlighted in Schenkel and Hart (2012) and Zick and Matyas (2015). Schenkel and Hart (2012) found that majority of the reanalysis data sets poorly resolve TC location and intensity. LaRow (2013) used the Center for Ocean-Atmospheric Prediction Studies (COAPS) Land-Atmosphere Regional Reanalysis for the Southeast (CLARReS10) (Stefanova et al., 2012) at 10-km grid interval to study landfalling TCs for the years 1979–2000 and found that near-surface winds were inadequately resolved when compared to the observed data. Similarly, Jourdain et al. (2014) investigated oceanic responses to TC surface winds by extracting wind data from ECMWF operational analysis and ERA-Interim reanalysis. They found that TC surface winds, on average, grossly underestimated intensity parameters causing misrepresentation of vertical mixing and Ekman pumping in the cold wake of the TC passage in the global eddy-permitting ocean reanalyses that were utilized.

Our motivation in this research is to examine the usability of a well-known sea-surface wind analysis data set like the National Aeronautics and Space Administration's (NASA) funded Cross-Calibrated Multi-Platform Ocean Surface Wind Vector L3.0 First-Look Analysis (hereafter referred CCMP) (Atlas et al., 2011) for TC application studies. For this study, we have used the metric of integrated kinetic energy (IKE) (Powell & Reinhold, 2007) to examine the fidelity of TC features in CCMP. IKE is the volume integral of the square of the surface winds from the radii of maximum winds (RMW) to gale-force strength (17 m/s or 34 kt; 1 kt ≈ 0.5 m/s) (Misra, DiNapoli, & Powell, 2013; Powell & Reinhold, 2007). IKE emphasizes on the spatial distribution of the surface winds around the TC unlike other metrics that overemphasize the peak sustained winds measured at a particular point and completely neglect the size of the TC (Franklin, Black, & Valde, 2003; Nolan, Zhang, & Uhlhorn, 2014). For example, accumulated cyclone energy (Bell et al., 2000) causes overestimation of seasonal TC activity because it uses only the point measurement of peak sustained winds (Yu & Chiu, 2012; Yu, Chou, & Chiu, 2009). Furthermore, Powell and Reinhold (2007) suggest that IKE represents the destructive potential of a TC far better than other metrics as the kinetic energy of the surface wind scales with wind loads on structures and also scales with the surface wind stress over ocean surface that force storm surge. The objective of this study is to validate IKE of the Atlantic TCs in the CCMP analysis and assess its usability for TC IKE diagnostic studies.

A brief discussion on the data sets used in this study is provided in section 2. We present our methodologies to perform our validation of IKE from CCMP in section 3. Section 4 discusses the results with final conclusions in section 5.

2 | DATA SETS

2.1 | The extended best-track data set

The Colorado State University extended best-track (EBT) data set (Demuth, DeMaria, & Knaff, 2006) provide wind radii data for TCs in the North Atlantic (NA) basin for the 1988–2015 period. From 1988 to 2003, the EBT wind radii were copied from the operational estimates found in the automated tropical cyclone forecast (ATCF) data files. In 2004, the wind radii became a formal best-tracked quantity in HURDAT2. Since 2004, the EBT wind radii use these values. Similarly, RMW in EBT is also from the operational estimates of the a-decks in the ATCF system. However, unlike the intensity and position parameters in HURDAT2 the RMW through the entire period are simply operational estimates and are not subject to post-season best-track analysis (Landsea & Franklin, 2013). In fact, Vigh, Knaff, and Schubert (2012) have pointed to significant inconsistencies between aircraft measurements of RMW and outer wind radii with those reported in EBT. Furthermore, Landsea and Franklin (2013) indicate that these wind radii estimates have an uncertainty range of 25–52% depending on its operational data source (which includes ship and buoy, aircraft, satellite-based estimates and operational analyses). Nonetheless, Knaff, Slocum, Musgrave, Sampson, and Strahl (2016) and Dolling, Ritchie, and Scott Tyo (2016) have indicated that these wind radii estimates are reasonable to use for method development studies despite their prevailing uncertainties. Furthermore, the EBT wind radii data have now been extended for a limited time period (2001–present) to the East Pacific basin (http://rammb.cira.colostate.edu/research/tropical_cyclones/tc_extended_best_track_dataset/). We will explore the IKE analysis of TCs in other tropical ocean basins in a future study. However, for this study we will be confined to the NA basin.

2.2 | CCMP winds

The CCMP analysis provides sea surface winds at a height of 10 m around the globe with the exception of the Arctic Ocean (Atlas et al., 2011). It has been widely used for a number of ocean related studies (Oey, Chang, Chang, Lin, & Xu, 2013; Zheng, Pan, & Li, 2016) including TC studies (Pei, Zhang, & Chen, 2015; Vukicevic, Uhlhorn, Reasor, & Klotz, 2014; Zhang, Pei, & Chen, 2013). The CCMP surface wind analysis version 1.1 (https://podaac.jpl.nasa.gov/dataset/CCMP_MEASURES_ATLAS_L4_OW_L3_0_WIND_VECTORS_FLK) is available at 0.25° grid spacing at 6-hourly intervals from 1987 to 2011. This analysis has been developed using the variational analysis method (VAM) (Hoffman et al., 2003) that combines in situ, remotely sensed observations (microwave radiometers and scatterometers; e.g., WindSat and QuikScat, respectively) and first guess estimate from analyses (ECMWF reanalysis [ERA-40] was used for 1987–1998 period and ECMWF operational analysis thereafter). Satellite-retrieved surface winds from the remote sensing systems (RSS) are derived after inter-calibrating the radiometers at a brightness temperature level to within 0.2 °C by using a refined sea surface emissivity model and a radiative transfer function (Atlas et al., 2011). This results in these wind retrievals being highly consistent across the different microwave radiometer platforms (e.g., SSM/I, SSMIS, AMSR, TMI, WindSat and GMI). In addition, both the scatterometer and radiometer data are validated against the ocean moored buoys that exhibit agreements to within 0.8 m/s. The VAM using the ERA-40 analysis as the background wind field assimilates the RSS instrument data with the moored ocean buoy measurements to produce the CCMP surface wind analysis referenced at a height of 10 m above the surface.

3 | METHODOLOGY

The definition of (total) IKE following Powell and Reinhold's (2007) is:

$$\mathrm{IKE}=\frac{1}{2}\int_h\int_{r_{\mathrm{MW}}}^{r_{\mathrm{XX}}}\int_0^{2\pi}\rho r V^2 d\alpha dr dz, \tag{1}$$

where ρ is a constant value for air density, which is taken to be 1.15 kg/m^3, V is the surface wind speed and the integration is a volume integral of the surface winds for a thickness of 1 m (h) between the observed RMW (r_{MW}) and radii of gale force winds (r_{xx}) 17 m/s or 34 kt) and α is the sector angle. Misra et al. (2013) developed a historical IKE data set for the NA TCs using EBT for the years 1990–2011, which is now extended to 2014. Because the data available from EBT are not gridded but available for the four quadrants of the TC, Misra et al. (2013) have suggested a detailed algorithm to compute IKE from such discrete data (Table 1). This data set will be used as the validation data set when comparing CCMP-IKE values. We separated the total IKE (Equation (1)) from EBT into three components (34, 50 and 64-kt IKE) for further comparison. In other words, we partitioned total IKE into IKE_{34-50}, IKE_{50-64} and $\mathrm{IKE}_{64\text{-RMW}}$ discretely as the sum of the square of the winds between 34 and 50 kt, 50 and 64 kt and 64 kt and RMW, respectively, from both EBT and CCMP data sets (following Equation 2). It should be noted that the EBT considers the asymmetries in the surface wind structure of the TC by providing estimates of wind radii in the primary intercardinal directional (northeast, southeast, southwest and northwest) quadrants of the TC at each fix and further we follow the algorithm provided in Table 1 following Misra et al. (2013). However, CCMP being a gridded analysis (albeit at 0.25° spatial resolution) provides an opportunity for a more accurate account of TC surface wind asymmetries than EBT.

It is well known that the size of the TC has a stronger bearing on IKE than the peak sustained wind speeds (Kozar & Misra, 2014; Misra et al., 2013; Musgrave, Taft, Vigh, McNoldy, & Schubert, 2012; Powell & Reinhold, 2007). Therefore, the size (or spatial extent) of the 34 kt winds for TCs plays a significant role in the total IKE than the comparatively smaller spatial extent of the 50 and 64 kt winds (Kozar & Misra, 2014). We therefore also computed separately IKE_{34-50}, IKE_{50-64} and $\mathrm{IKE}_{64\text{-RMW}}$ from CCMP analysis to validate with corresponding IKE derived from EBT data. These were computed as:

$$\mathrm{IKE}_{r_{\mathrm{XX}}-r_{\mathrm{YY}}}=\frac{1}{2}\int_h\int_{r_{\mathrm{YY}}}^{r_{\mathrm{XX}}}\int_{\theta_{\mathrm{CCMP}};\mathrm{EBT}}\rho r V^2 d\alpha dr dz, \tag{2a}$$

where r_{xx} and r_{yy} refers to the radii for one of the four wind speeds (34 kt, 50 kt, 64 kt and $V_{\max}$) and the differing limits of integration of $d\alpha$ owing to the difference in the discretization of the two data sets (CCMP and EBT) would therefore follow as:

$$\theta_{\mathrm{CCMP}}=0<\alpha<2\pi, \tag{2b}$$

$$\theta_{\mathrm{EBT}}=\begin{cases}0<\alpha<\dfrac{\pi}{2}, \text{ as } \theta_1 \text{ in the first quadrant}\\ \dfrac{\pi}{2}<\alpha<\pi, \text{ as } \theta_2 \text{ in second quadrant}\\ \pi<\alpha<\dfrac{3\pi}{2}, \text{ as } \theta_3 \text{ in third quadrant}\\ \dfrac{3\pi}{2}<\alpha<2\pi, \text{ as } \theta_4 \text{ in fourth quadrant}\end{cases}. \tag{2c}$$

For example, EBT IKE computed between 34 and 50 kt winds will be computed as:

$$\mathrm{IKE}_{34-50}=\frac{1}{2}\int_h\left\{\int_{r_{50}}^{r_{34}}\int_{\theta_1} rV^2 d\alpha dr+\int_{r_{50}}^{r_{34}}\int_{\theta_2} rV^2 d\alpha dr\right.$$
$$\left.+\int_{r_{50}}^{r_{34}}\int_{\theta_3} rV^2 d\alpha dr+\int_{r_{50}}^{r_{34}}\int_{\theta_4} rV^2 d\alpha dr\right\}dz. \tag{3a}$$

It may be noted that the above sectoral area integrals within the curly brackets in Equation 3a are discretely computed following the algorithm outlined in Table 1. However,

TABLE 1 Algorithm to compute IKE from EBT wind radii data (adapted from Misra et al., 2013)

Annulus contribution to IKE	Condition	Mean wind (kt)	Area
IKE_{34-50}	$R_{50} > 0$	40	1/4 $\pi(R_{34}^2-R_{50}^2)$
	No R_{50}, $V_{\max} > 50$, $R_{34} >$ RMW	40	1/4 $\pi(R_{34}^2-[0.75\mathrm{RMW}]^2)$
	No R_{50}, $V_{\max} < 50$, $R_{34} >$ RMW	1/4 $V_{\max}$ + 3/4 (34)	1/4 $\pi(R_{34}^2-[0.75\mathrm{RMW}]^2)$
	No R_{26}, RMW = R_{34}	34	1/4 $\pi(R_{34}^2-[0.5R_{34}]^2)$
IKE_{50-64}	$R_{64} > 0$	27.75	1/4 $\pi(R_{50}^2-R_{64}^2)$
	No R_{64}, $V_{\mathrm{MS}} > 64$, $R_{50} >$ RMW	27.75	1/4 $\pi(R_{50}^2-[0.75\mathrm{RMW}]^2)$
	No R_{64}, $V_{\max} < 64$, $R_{50} >$ RMW	0.25 $V_{\max}$ + 0.75 (50)	1/4 $\pi(R_{50}^2-[0.75\mathrm{RMW}]^2)$
	No R_{64}, $R_{50} \leq$ RMW	26	1/4 $\pi(R_{50}^2-[0.5\mathrm{R}_{50}]^2)$
$\mathrm{IKE}_{>64}$	Max R_{64} quadrant, $R_{64} >$ RMW	0.25 $V_{\max}$ + 0.75 (64)	1/4 $\pi(R_{64}^2-[0.75\mathrm{RMW}]^2)$
	Max R_{64} quadrant, R_{64} = RMW	0.25 $V_{\max}$ + 0.75 (64)	1/4 $\pi(R_{64}^2-[0.75R_{64}]^2)$
	$R_{64} <$ RMW	0.1 $V_{\max}$ + 0.9 (64)	1/4 $\pi(R_{64}^2-[0.75R_{64}]^2)$
	Not max R_{64} quadrant, RMW = R_{64}	0.1 $V_{\max}$ + 0.9 (64)	1/4 $\pi(R_{64}^2-[0.75\mathrm{RMW}]^2)$

$V_{\max}$ = maximum sustained wind speed.

TABLE 2 The correlation of IKE with wind radii from EBT data (Demuth et al., 2006) for three different time periods

	All years (1990–2014)	Non-best-track years (1990–2003)	Best-track years (2004–2014)
34 kt radii	.91	.92	.93
50 kt radii	.83	.84	.84
64 kt radii	.68	.65	.73

in the gridded data set of CCMP, IKE computed for example, between 34 and 50 kt winds will be:

$$\mathrm{IKE}_{34-50} = \frac{1}{2}\int_h \int_{r_{50}}^{r_{34}} \int_0^{2\pi} \rho r V^2 d\alpha dr dz. \quad (3b)$$

This difference in methodology of computing IKE from a gridded analysis like CCMP (using Equation 3b) and from data set like EBT (Equation 3a) is apparent.

However, we quickly found that CCMP poorly resolves 50 and 64 kt winds in TCs of the NA basin. In fact, of the 1,414 and 979 fixes of TCs that had 50 and 64 kt winds in the EBT data (for the period 2004–2011) there were only 289 and 218 fixes in the corresponding CCMP analysis, respectively. Therefore, given such poor capture and small sample size of the TC wind structure at high wind speeds, we have limited our discussion of the verification results to only the IKE_{34-50} of TCs in the CCMP analysis.

Table 2 clearly shows that the 34 kt radii variation explains more variance of the total IKE than the radii of the other two specified wind regimes in the EBT data. It may be noted that all correlation values in Table 2 pass the 5% significance level according to *t* test. Furthermore, the choice of the time period (exclusively using best-track years vs. non-best-track years of EBT) chosen has the least impact on this relationship for all three wind speed ranges (Table 2).

In order to understand the methodological differences in the diagnosis of IKE between EBT and CCMP IKE, we computed IKE in CCMP using both Equations 3a and b. It may be noted that we diagnosed the maximum radial extent of 34 kt winds in each of the four quadrants before using Equation 3a for the CCMP data set. Figure 1 shows the difference in IKE estimates from the two methodologies (Equations 3a and b) for all TC fixes in the CCMP data set that resolved 34 kt winds or higher in at least one of the quadrants. It is clearly seen from this figure that Equation 3a overestimates IKE relative to Equation 3b. For the sake of consistency in verifying with EBT IKE we choose to use Equation 3a to compute CCMP IKE even though the use of Equation 3b would provide a more representative estimate of IKE for a given TC fix in a gridded analysis like the CCMP data set.

4 | RESULTS

4.1 | Validation of CCMP surface wind analysis

The EBT data set contains 2,353, 6-hourly time fixes of TCs with IKE_{34-50} values for the years 2004–2011. However, CCMP only resolved 514 fixes out of the aforementioned 6-hourly time fixes with 34 kt wind radii. Atlas et al. (2011) clearly indicate that all microwave sensors used in the CCMP analysis are sensitive to rain with increasing rain rate associated with decreased accuracy. Furthermore, data gaps of satellite-retrieved winds can also result in such poor validation. A scatter plot between CCMP's resolved IKE_{34-50} against EBT's IKE_{34-50} (Figure 2a) and EBT's total IKE (Figure 2b) displays the fidelity of the CCMP wind structure of NA TCs. It may be noted that in Figure 2a,b there are only 514 TC fixes resolved by CCMP analysis. The explained variance of CCMP's IKE_{34-50} on the corresponding EBT's IKE_{34-50} ($R^2 = 31\%$) in Figure 2a is similar to that for total IKE from EBT ($R^2 = 32\%$;

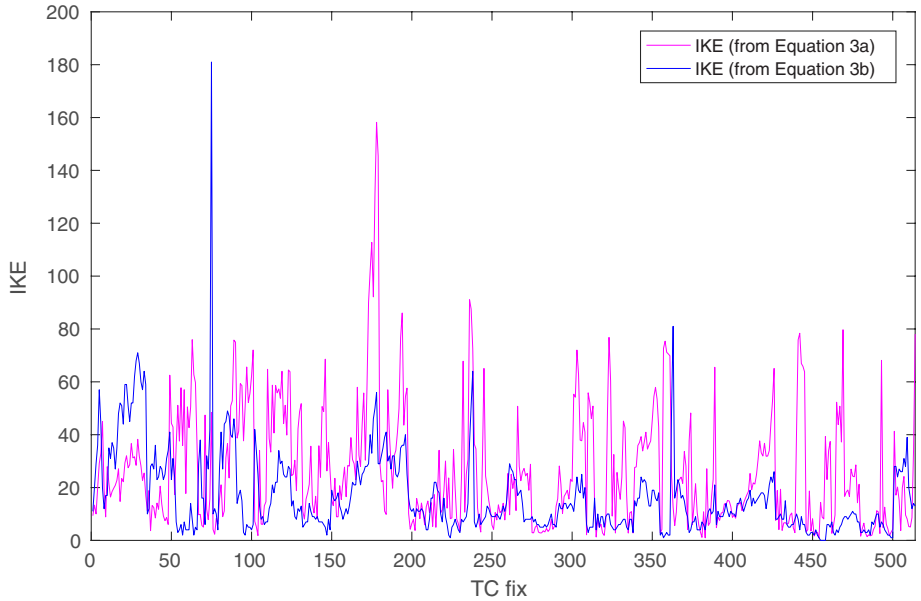

FIGURE 1 IKE (in TJ) computed from Equations and from CCMP data sets for all 514 TC fixes in which 34 kt or greater wind speed was resolved [Colour figure can be viewed at wileyonlinelibrary.com]

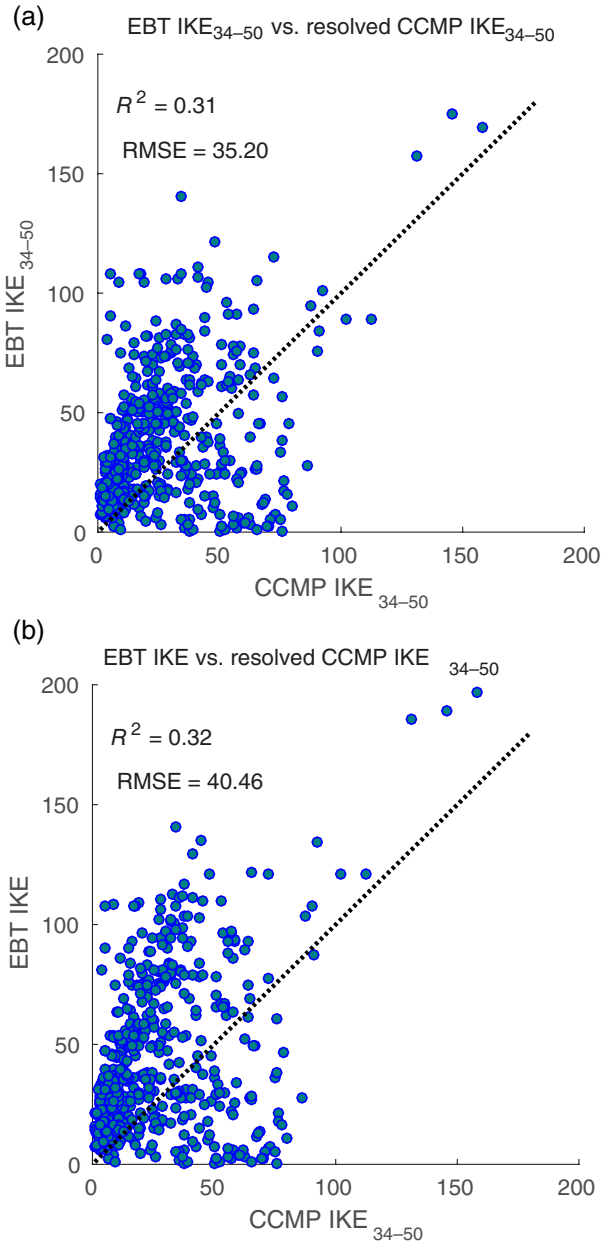

FIGURE 2 Scatter of IKE (in Terra Joules; TJ) from CCMP surface wind analysis (Atlas et al., 2011) with corresponding EBT data (Demuth et al., 2006) for Atlantic TCs from 2004–2011. (a) Scatter shows the spread of EBT $IKE_{34–50}$ vs. the CCMP $IKE_{34–50}$ (Equation 3a). (b) Scatter of EBT total IKE (Equation (1)) vs. CCMP $IKE_{34–50}$. The unit of RMSE is TJ. The dotted black line is $y = x$ line [Colour figure can be viewed at wileyonlinelibrary.com]

Figure 2b). The comparable values of R^2 value between Figure 2a,b suggest yet again that the radii of the 34 kt wind is critical for total IKE in the EBT data set. The majority of the points in the scatter plot of Figure 2a lie above the diagonal line ($y = x$) suggesting that there is a systematic underestimation of IKE from CCMP relative to EBT. There is however a significant minority of fixes (with IKE ranging up to about 100TJ) for which CCMP overestimates IKE relative to the EBT data set. Similarly, Figure 2b also shows that $IKE_{34–50}$ from CCMP underestimates the total IKE from EBT for a majority of TC fixes with IKE <100TJ. The relatively large RMSE values in Figure 2a,b reemphasize the bias in the CCMP TC wind structure.

The climatological seasonal cycle of the number of TCs and $IKE_{34–50}$ computed over the period of 2004–2011 are shown in Figure 3a,b, respectively. The number of TCs in EBT data set in Figure 3a (2,279 over all seasons) correspond to TCs which had 34 kt wind reported at least in one quadrant in at least one 6-hourly fix over the lifetime of the TC. Similarly, the number of TCs in the CCMP data set in Figure 3a (505 over all seasons) are those in which the 34 kt wind radii is resolved in at least one 6-hourly fix over the lifetime of the TC. Figure 3a clearly shows that the CCMP systematically underestimates the number of fixes and the number of TCs throughout the NA season. In the months of August, September and October the differences in the count of both the TCs and the fixes between CCMP and EBT data sets are the largest (Figure 3a). In a related study, Misra et al. (2013) indicate that these are the months when TC's in the NA have the longest lifespans and acquire their largest size. Coincidentally, we also observe that the largest bias in CCMP IKE appear in August, September and October (Figure 3b). The IKE bias in the CCMP data set is so severe that even its seasonal cycle is not well represented. For example, CCMP shows a seasonal peak in July followed by the next maximum in November contrary to the EBT data set. We also compared the seasonal cycle of IKE for the same fixes in both CCMP and EBT data sets (i.e., for the 505 fixes of CCMP; not shown) and found the differences to be qualitatively very similar to Figure 3b. This indicates that at least the bias in the seasonal phase of IKE in the CCMP analysis in Figure 3b is largely from the bias in the TC size and its wind structure.

We also computed the track density expressed as the number of TCs per 2 × 2° cell with non-zero $IKE_{34–50}$ separately from both EBT and CCMP analysis (Figure 4). It may be noted that in Figure 4 TCs that stayed within one cell for multiple 6-hourly time fixes were counted as many times as they appeared in the cell. In examining Figure 4a–c, a number of features can be noted: (a) The overall track density across NA Ocean is generally far less in CCMP relative to EBT, (b) the track density differences are comparatively less in the Gulf of Mexico and near the Gulf coastal regions than those in central and eastern Atlantic Ocean (Caribbean Sea) and (c) the largest differences in track density are observed in the deep tropical Atlantic in the main development region (MDR) (10°–20°N, 80°–20°W) and in the subtropical latitudes including the Atlantic coast. The bias over the MDR suggests that CCMP has difficulty in resolving TC's at time of genesis when they are small in size and are also potentially short-lived. There are however other reasons for the differences between Figure 4a,b. For instance, there is a higher frequency of TC fixes in the open ocean in the EBT data than near the coasts, which then leads to the likelihood of more differences from CCMP data set over open oceans because of the sample size differences. Another reason is

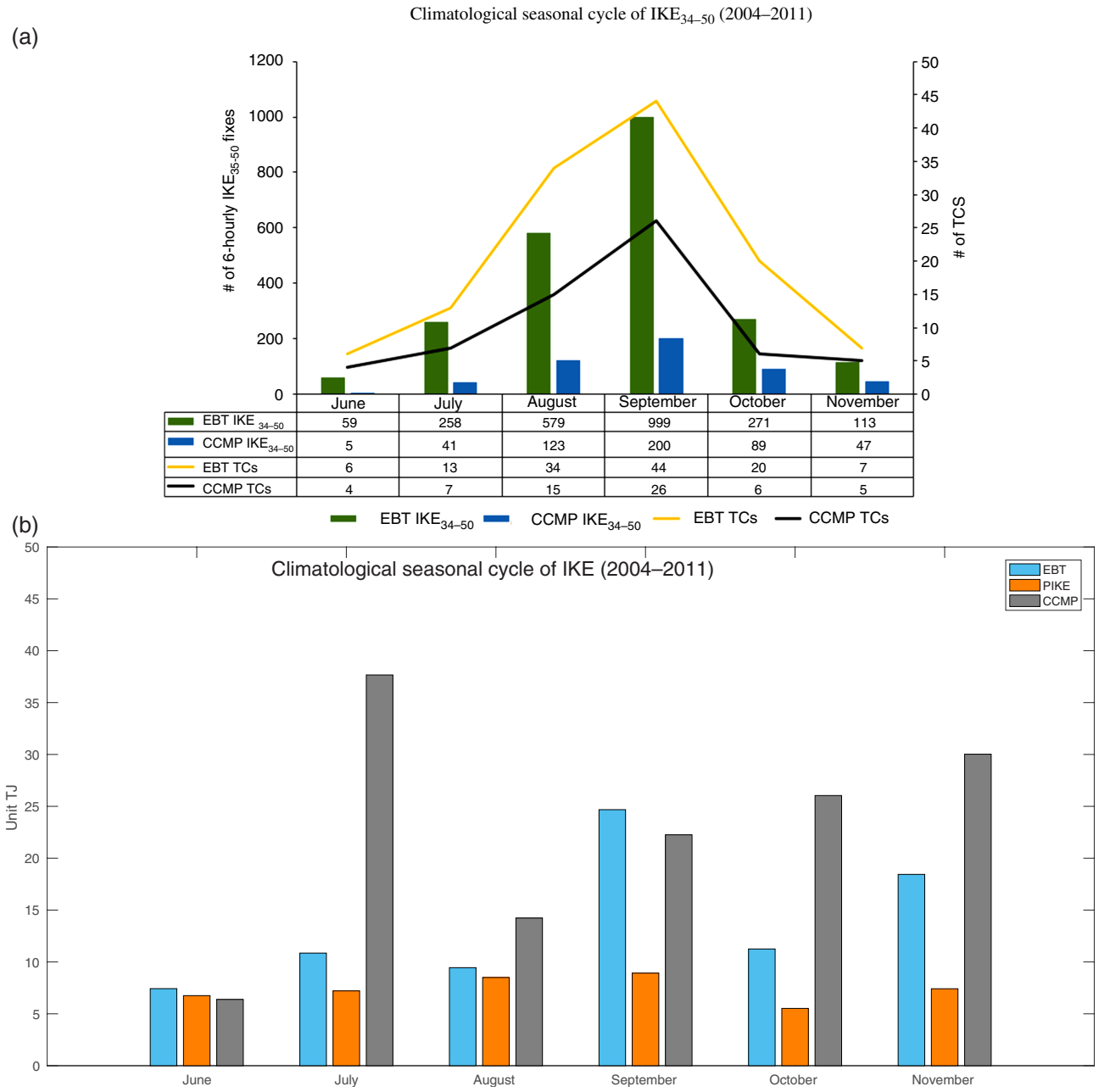

	June	July	August	September	October	November
EBT IKE 34–50	59	258	579	999	271	113
CCMP IKE34–50	5	41	123	200	89	47
EBT TCs	6	13	34	44	20	7
CCMP TCs	4	7	15	26	6	5

FIGURE 3 (a) Climatological seasonal cycle of the number of fixes used in computing IKE from EBT (green bar) and CCMP (blue bar) data sets. These fixes reported with 34 kt wind at least in one quadrant in the EBT or over one grid point in the CCMP data sets. Similarly, the number of TCs in the EBT (yellow line) and the corresponding number of resolved TCs in the CCMP (black line) are also shown. The numerical values of the number of fixes (in the first two rows) and number of TCs (in the bottom two rows) from EBT and CCMP data sets are indicated in the embedded table. (b) Climatological seasonal cycle of IKE (TJ) from EBT (blue bar), CCMP (grey bar) and ProxyIKE (TJ; PIKE; orange bar) computed from CCMP data set. Because the sample sizes in CCMP and EBT data set are so disparate, we used the median IKE values for each month to reduce the influence of the different sample size on the climatological seasonal cycle of IKE [Colour figure can be viewed at wileyonlinelibrary.com]

that in the open ocean CCMP analysis relies more heavily on remotely sensed wind that is contaminated by rain clouds of the TC and therefore results in less coverage of TC winds by CCMP analysis (Atlas et al., 2011).

4.2 | The proxy IKE in CCMP analysis

Given the relatively poor validation of the TC wind structure in the CCMP analysis especially for the smaller-sized TCs, we resort to the development of a proxy IKE (PIKE), which is defined as the contour integral of the product of the square of the winds at the radius of the last closed isobar (ROCI) and the radius of the last closed isobar (r_{ROCI}). The concept of PIKE is fundamentally motivated by the fact that IKE is more dependent on the size of the TC than its maximum sustained wind speed. Mathematically, PIKE may be expressed as:

$$\mathrm{PIKE} = \int_h \oint_{r_{\mathrm{ROCI}}}^{r_{\mathrm{ROCI}}} \rho r_{\mathrm{ROCI}} V_{\mathrm{ROCI}}^2 dcdz. \quad (4)$$

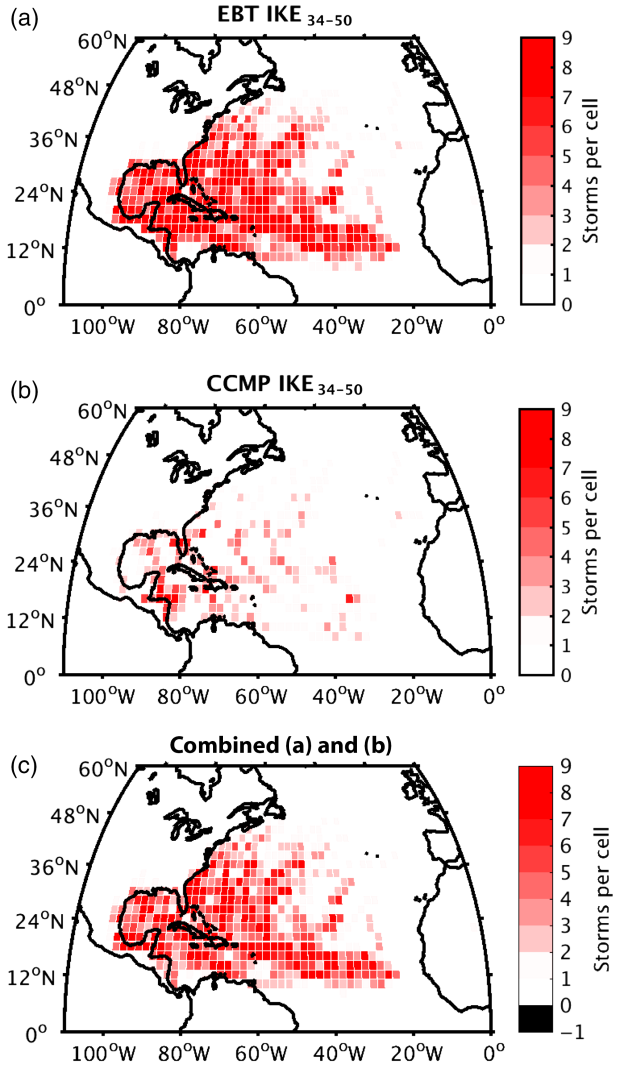

FIGURE 4 The composite track density (number of TCs based on non-zero values of IKE_{34-50} per 2 × 2° cell) plot of NA TCs for the years 2004–2011 from (a) EBT, (b) CCMP and (c) combined (a) and (b). The grid cells are of equal area, normalized by the cosine of latitude [Colour figure can be viewed at wileyonlinelibrary.com]

Equation 4 suggests that PIKE is the kinetic energy based on winds at ROCI (V_{ROCI}) that is integrated along the contour of r_{ROCI}. Further motivation to develop PIKE is the increased likelihood of resolving the winds at ROCI in CCMP analysis because of its weaker wind speeds and larger size than radii of winds stronger or equal to tropical storm strength. In addition, the relative distance of ROCI from the very active areas of convection around the centre of the TC and along the surrounding rain bands would make the diagnosis of the winds less susceptible to contamination from precipitating clouds in the CCMP analysis. Furthermore, PIKE from CCMP analysis provides the likelihood for better verification with IKE from EBT data because IKE is far more sensitive to the size of the TC than wind speed (Misra et al., 2013; Powell & Reinhold, 2007) and ROCI is a good measure of the size of the TC (Carrasco, Landsea, & Lin, 2014).

Very importantly we are able to compute PIKE for all 2,353 TC fixes in the EBT data set for which IKE was computed. This is because PIKE is designed to capture the variations of IKE based on winds at ROCI and does not require TC in CCMP to acquire tropical storm strength winds or higher. In comparison, it may be noted that the CCMP analysis resolved only 21.8, 20 and 22% of the TC fixes with 34, 50 and 64 kt wind radii TC's relative to EBT data, respectively. The seasonal cycle of PIKE is slightly improved over that of CCMP (Figure 3b) with at least the seasonal peak appearing in September as in EBT data set. However, PIKE underestimates EBT IKE in every month of the season significantly. This bias is expected given that PIKE is purely based on winds at ROCI which would be much weaker than the tropical storm strength or higher wind speeds. The largest bias of PIKE appears in September and November while the smallest bias is displayed in June followed by August (Figure 3b). This suggests that PIKE

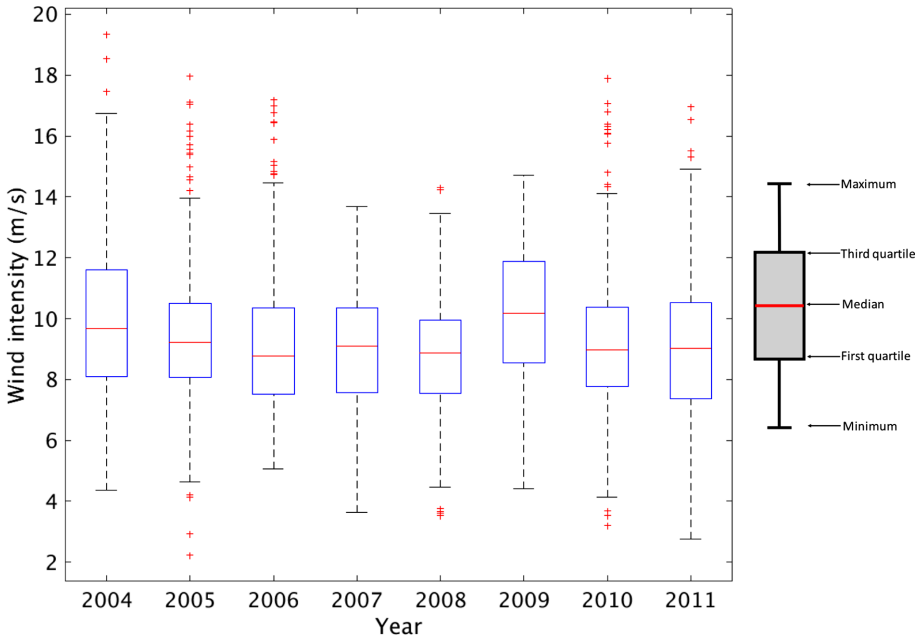

FIGURE 5 Boxplot depicting the distribution of the magnitude of the wind speed at ROCI in CCMP wind analysis. The index for the boxplot is shown in the far top right. The outliers are shown by the red + signs [Colour figure can be viewed at wileyonlinelibrary.com]

displays greater benefit over CCMP IKE for small-sized TCs that typically are observed in early part of the Atlantic hurricane season. The bias in PIKE begins to increase substantially in the months when large-sized TCs with associated asymmetries, are more prevalent during the seasonal peak and towards the end of the season. The asymmetries cause distortion of the ROCI from a symmetric single value provided by EBT for each TC fix. As a result, PIKE is bound to develop a bias for such TCs.

A display of the distribution (boxplot) of the winds at ROCI (Figure 5) indicates that the median wind at ROCI—for all 8 years of study—is around 9.2 m/s with maximum winds near gale-force strength in some of the years (e.g., 2004, 2009 and 2011). These comparatively strong winds at ROCI are usually on account of the asymmetric features from the extratropical transition of a relatively large-sized TC (Evans & Hart, 2003; Kimball & Mulekar, 2004). Furthermore, it should be noted that ROCI is affected by the translation speed of the TC, which makes its estimate fairly difficult and uncertain (Merrill, 1984; Chu, Sampson, Levine, & Fukada, 2002; Cocks & Gray, 2002). In addition, the pressure of the last closed isobar in EBT takes on discrete integer values of 1 hPa and ROCI could vary a fair amount over that interval. Therefore, the wind speeds at ROCI could have substantial variance as indicated in Figure 5. Finally, some subjectivity exists in estimates of ROCI especially when last closed isobar is distorted (Cocks & Gray, 2002).

The scatter between IKE from EBT and PIKE computed from CCMP wind analysis at ROCI is shown in Figure 6a

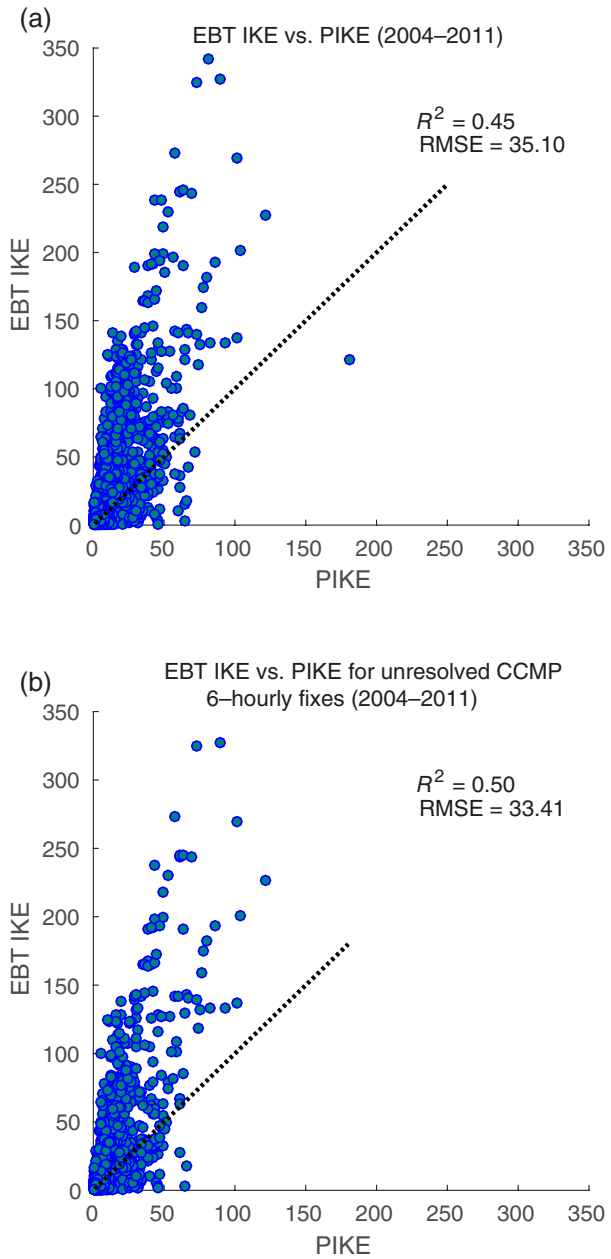

FIGURE 6 The scatter between PIKE (Equation 4; TJ) based on surface winds from CCMP winds and total EBT IKE (Equation (1); TJ) for (a) all fixes in the EBT data and (b) for TC fixes with at least tropical storm strength winds in EBT data that is unresolved in CCMP analysis. The dotted black line in both panels is $y = x$ line [Colour figure can be viewed at wileyonlinelibrary.com]

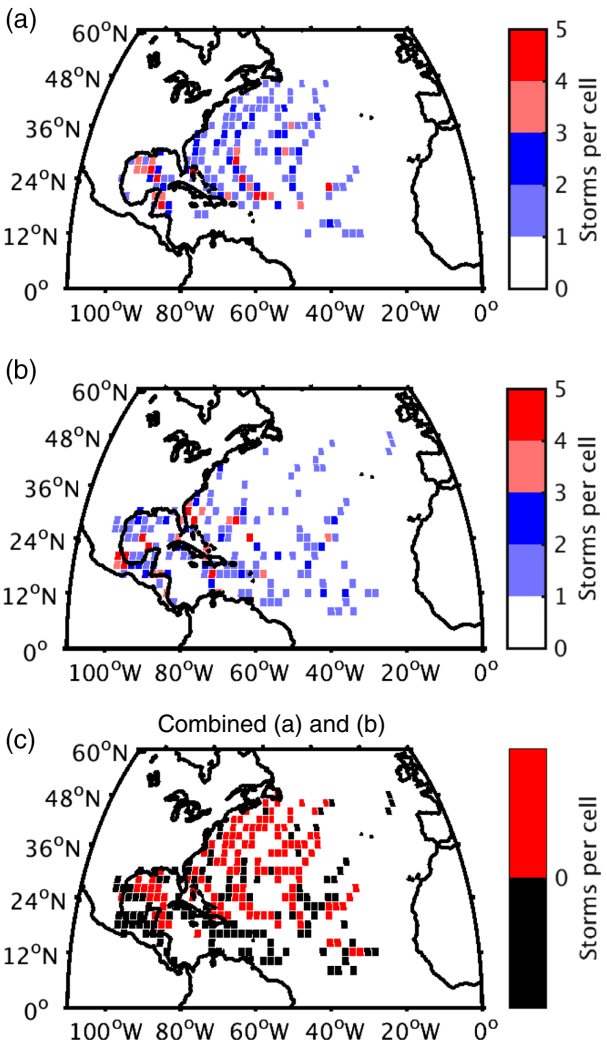

FIGURE 7 The composite track density (number of TCs per 2 × 2° cell) plot of TCs for which the PIKE from CCMP validates most (a) poorly, (b) closely (see text for explanation) and (c) combined (a) and (b) with corresponding IKE of TCs from EBT for the 2,353 fixes between the years 2004 and 2011. The grid cells are of equal area, normalized by the cosine of latitude [Colour figure can be viewed at wileyonlinelibrary.com]

for all 2,353 TC fixes between 2004 and 2011, which indicates a correlation of .67 (or $R^2 = .45$) and RMSE value of 35.10 TJ. In comparison, the conventional IKE computed from the CCMP wind analysis for all 2,353 fixes of EBT data set displayed a correlation of .56 (or $R^2 = .32$) and RMSE value of 40.46 TJ (Figure 2b). The improvement of PIKE is further corroborated in Figure 6b, which shows the scatter of PIKE and IKE from EBT exclusively for TC fixes with tropical storm strength winds that were not resolved by CCMP analysis. Here the correlation between PIKE and IKE is .71 ($R^2 = .50$) and RMSE is 33.41 TJ.

A composite track density of TC fixes falling at or below the 10th and at or above the 90th percentile of absolute difference between IKE and PIKE (|IKE − PIKE|) to represent the most closely and poorly validated estimates of IKE from PIKE are shown in Figure 7a,b with their difference in Figure 7c, respectively. The value for the 10th (90th) percentile in absolute difference is 0.92 TJ (55.67 TJ). In examining Figure 7a–c, we see some overlap in the geographical location of the TC fixes whose PIKE value most poorly and closely validate EBT IKE. There is however a subtle difference with more recurving TCs and TCs with a northerly track (likely undergoing extratropical transition) validating more poorly (Figure 7a) than the relatively zonally tracking TCs of the deep tropics (Figure 7b). One of the explanations for this difference is the higher values of IKE for larger-sized extratropical cyclones (Misra et al., 2013) that increases the likelihood increased magnitude of errors in the estimates of IKE from PIKE relative to EBT derived IKE values. Furthermore, increasing asymmetries in the wind structure as TCs undergo extratropical transition (Evans & Hart, 2003) result in reducing the validity of using a symmetric estimate for ROCI obtained from EBT. In addition, estimating ROCI where the last closed isobar is distorted (which is likely to be the case for TC undergoing extratropical transition) in itself is uncertain. These factors are likely to increase the discrepancy between PIKE from CCMP and IKE from EBT especially for such asymmetric TCs.

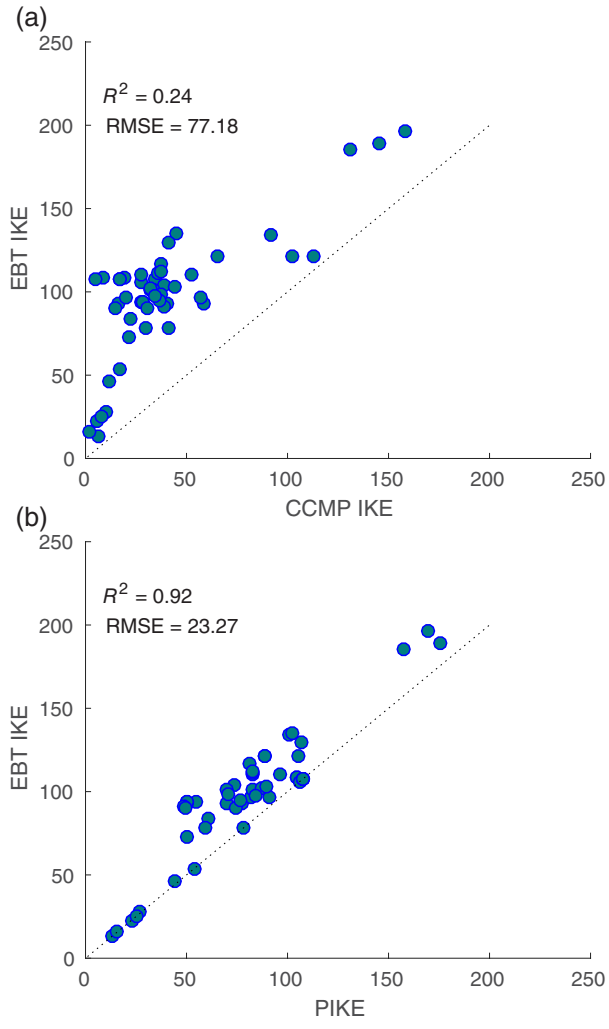

FIGURE 8 The scatter between EBT IKE (TJ) and (a) CCMP IKE (TJ) and (b) PIKE (TJ) for fixes that are at or above the 90th percentile of differences between PIKE and EBT IKE. The dotted black line represents $y = x$ line [Colour figure can be viewed at wileyonlinelibrary.com]

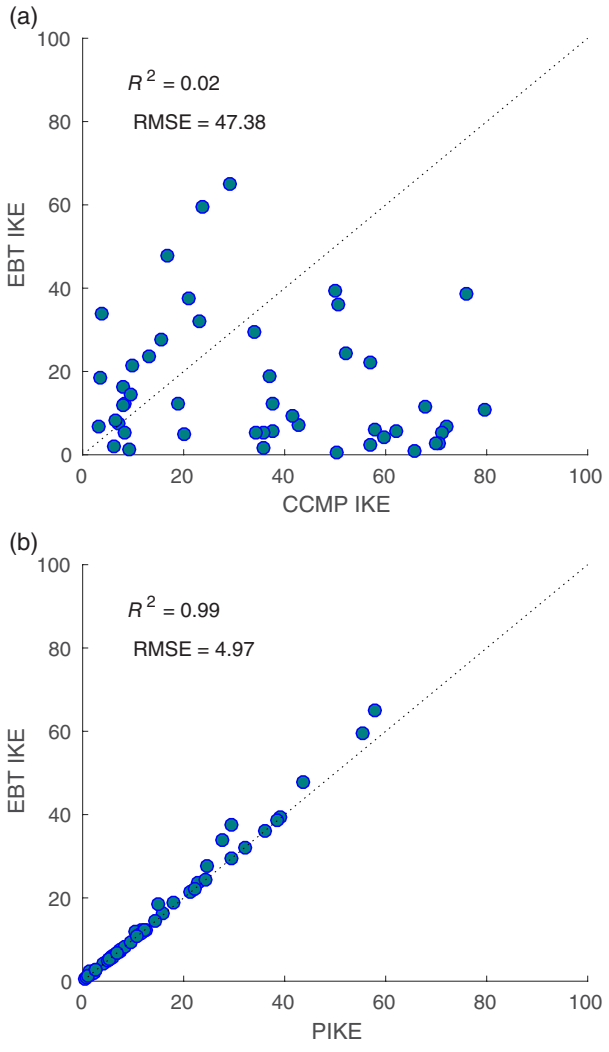

FIGURE 9 The scatter between EBT IKE (TJ) and (a) CCMP IKE (TJ) and (b) PIKE (TJ) for fixes that are at or below the 10th percentile of differences between PIKE and EBT IKE. The dotted black line represents $y = x$ line [Colour figure can be viewed at wileyonlinelibrary.com]

We also show the scatter of the EBT IKE with PIKE and CCMP IKE for the fixes for which PIKE verified poorly (fixes at 90th percentile or above for the difference between PIKE and EBT IKE; Figure 8) and reasonably (fixes at 10th percentile or below for the difference between PIKE and EBT IKE; Figure 9). In both these instances, we clearly see that PIKE outperforms CCMP IKE. It is quite clear from all of this analysis that PIKE is a good alternative to IKE in the CCMP data set. In comparing Figures 8 and 9 it is clear that PIKE verifies better with EBT IKE in instances of TC with smaller IKE.

5 | CONCLUSIONS

The aim of the article was to examine the fidelity of the TC-IKE over several hurricane seasons of the tropical NA in the CCMP analysis. We used the EBT data for validation. IKE relies on the structure of specified surface wind regimes, which makes it a reliable metric to estimate potential damage from storm surge and wind load on structures. Because IKE is not dependent on a transient feature like the peak sustained wind speed but volume integrates the surface wind from the centre of the TC out to 34 kt wind speed, it has considerable inertia and therefore has the potential to be simulated or predicted better than other TC metrics (Kozar & Misra, 2014; Kozar, Misra, & Powell, 2016). It should be noted however that the observed wind radii estimates from EBT have considerable uncertainty, which makes any validation exercise of IKE challenging. However, it is imperative to pursue these studies despite the limitations of observations given the growing recognition of the importance of TC size and IKE on the potential impacts of landfalling TCs.

The CCMP analysis was found to barely resolve 34 kt winds in the majority of TCs let alone winds at 50 and 64 kt wind reported in EBT. We therefore computed $IKE_{34–50}$ from the CCMP wind analysis, which only resolved 21.8% of comparable fixes in EBT. It was found that $IKE_{34–50}$ from CCMP analysis was found to explain about 30% of the variance of the total IKE in the EBT data for the NA basin for the resolved TC fixes in the CCMP analysis. The CCMP analysis was also found to particularly have issues of IKE bias in TCs that were small in size and short in lifespan. In many such cases, CCMP failed to resolve the TC fixes. Large TCs with long lifespans are invariably resolved in the CCMP irrespective of their location (either in the open ocean or near the coast). But the areal coverage of gale-force winds for large TCs were also underestimated in the CCMP analysis relative to the EBT data set giving rise to large errors in the estimates of IKE. The climatological seasonal cycle of $IKE_{34–50}$ for the NA TCs are also very poorly validated in the CCMP winds. The seasonal peak of IKE in CCMP appears in July which is contrary to the EBT data set that shows seasonal peak in September. Furthermore, CCMP also grossly underestimate total IKE and the number of fixes relative to EBT data.

A PIKE based on the volume integration of the square of the winds at the ROCI is introduced. PIKE from CCMP analysis shows promise in validating with EBT IKE. PIKE shows significant improvement over IKE from CCMP for a broad range of TC sizes. PIKE however displays larger bias for northwards tracking NA TC's. This may be a result of the increasing influence of wind asymmetries of larger-sized TCs that is not reasonably well represented in PIKE owing to symmetric single values of ROCI for each TC fix.

ACKNOWLEDGEMENTS

We thank Dr. Michael Kozar for sharing the code to compute IKE. We thank Dr. Jonathan Vigh and two anonymous reviewers for providing very useful suggestions on earlier versions of this manuscript. S.B. was supported by FSU IDEA grant support. This work was also supported by grants from NOAA (NA12OAR4310078) and USGS G13AC00408.

ORCID

Vasubandhu Misra http://orcid.org/0000-0002-1345-6280

REFERENCES

Atlas, R., Hoffman, R. N., Ardizzone, J., Leidner, S. M., Jusem, J. C., Smith, D. K., & Gombos, D. (2011). A cross-calibrated, multiplatform ocean surface wind velocity product for meteorological and oceanographic applications. *Bulletin of the American Meteorological Society*, *92*, 157–174. https://doi.org/10.1175/2010BAMS2946.1

Bell, G. D., Halpert, M. S., Kousky, V. E., Gelman, M. E., Ropelewski, C. F., Douglas, A. V., & Schnell, R. C. (2000). Climate assessment for 1999. *Bulletin of the American Meteorological Society*, *81*(6), S1–S50.

Carrasco, C., Landsea, C., & Lin, Y. (2014). The influence of tropical cyclone size on its intensification. *Weather and Forecasting*, *29*, 582–590.

Chu, J.-H., Sampson C. R., Levine A. S., & Fukada E. 2002. *The joint typhoon warning center tropical cyclone best-tracks, 1945–2000* (Ref. NRL/-MR/7540-02, p. 16). Retrieve from http://www.usno.navy.mil/NOOC/nmfc-ph/RSS/jtwc/best_tracks/TC_bt_report.html

Cocks, S. B., & Gray, W. M. (2002). Variability of the outer wind profiles of western North Pacific typhoons: classifications and techniques for analysis and forecasting. *Monthly Weather Review*, *130*(8), 1989–2005.

Demuth, J., DeMaria, M., & Knaff, J. A. (2006). Improvement of advanced microwave sounder unit tropical cyclone intensity and size estimation algorithms. *Journal of Applied Meteorology*, *45*, 1573–1581.

Dolling, K., Ritchie, E. A., & Scott Tyo, J. (2016). The use of the deviation angle variance technique on geostationary satellite imagery to estimate tropical cyclone size parameters. *Weather and Forecasting*, *31*(5), 1625–1642.

Evans, J. L., & Hart, R. E. (2003). Objective indicators of the life cycle evolution of extratropical transition for Atlantic tropical cyclones. *Monthly Weather Review*, *131*, 909–925.

Franklin, J. L., Black, M. L., & Valde, K. (2003). GPS dropwindsonde profiles in hurricanes and their operational implications. *Weather and Forecasting*, *18*, 32–44. https://doi.org/10.1175/1520-0434(2003)018,0032: GDWPIH.2.0.CO;2.

Hart, R., Maue, R., & Watson, M. (2007). Estimating the atmospheric and SST memory of tropical cyclones through MPI anomaly evolution. *Monthly Weather Review*, *135*, 3990–4005.

Hart, R. E. (2011). An inverse relationship between aggregate tropical cyclone activity and subsequent winter climate. *Geophysical Research Letts*, *38*, L01705. https://doi.org/10.1029/2010GL045612

Hoffman, R. N., Leidner, S. M., Henderson, J. M., Atlas, R., Ardizzone, J. V., & Bloom, S. C. (2003). A two-dimensional variational analysis method for NSCAT ambiguity removal: Methodology, sensitivity, and tuning. *Journal of Atmospheric Oceanic Technology*, *20*, 585–605.

Jourdain, N. C., Barnier, B., Ferry, N., Vialard, J., Menkes, C. E., Lengaigne, M., & Parent, L. (2014). Tropical cyclones in two atmospheric (re)analyses and their response in two oceanic reanalyses. *Ocean Modelling*, *73*, 108–122.

Kimball, S., & Mulekar, M. (2004). A 15-year climatology of North Atlantic tropical cyclones, part 1: Size parameters. *Journal of Climate*, *17*, 3555–3575.

Knaff, J. A., Slocum, C. J., Musgrave, K. D., Sampson, C. R., & Strahl, B. R. (2016). Using routinely available information to estimate tropical cyclone wind structure. *Monthly Weather Review*, *144*(4), 1233–1247. https://doi.org/10.1175/MWR-D-15-0267.1

Kozar, M. E., & Misra, V. (2014). Statistical prediction of integrated kinetic energy in North Atlantic tropical cyclones. *Monthly Weather Review*, *142*, 4646–4657.

Kozar, M. E., Misra, V., & Powell, M. (2016). Hindcasts of integrated kinetic energy in Atlantic tropical cyclones: A neural network prediction scheme. *Monthly Weather Review*, *144*, 4591–4603. https://doi.org/10.1175/MWR-D-16-00301.1.

Landsea, C. W., & Franklin, J. L. (2013). Atlantic hurricane database uncertainty and presentation of a new database format. *Monthly Weather Review*, *141*, 3576–3592.

LaRow, T. (2013). An analysis of tropical cyclones impacting the southeast United States from a regional reanalysis. *Regional Environmental Change*, *13*(S1), 35–43.

Merrill, R. T. (1984). A comparison of large and small tropical cyclones. *Monthly Weather Review*, *112*(7), 1408–1418. https://doi.org/10.1175/1520-0493

Misra, V., DiNapoli, S., & Powell, M. (2013). The track integrated kinetic energy of Atlantic 615 tropical cyclones. *Monthly Weather Review*, *141*(7), 2383–2389.

Musgrave, K. D., Taft, R. K., Vigh, J. L., McNoldy, B. D., & Schubert, W. H. (2012). Time evolution of the intensity and size of tropical cyclones. *Journal of Advances in Modeling Earth Systems*, *4*, M08001.

Nolan, D., Zhang, J. A., & Uhlhorn, E. W. (2014). On the limits of estimating maximum wind speeds in hurricanes. *Monthly Weather Review*, *142*, 2814–2832.

Oey, L.-Y., Chang, M.-C., Chang, Y.-L., Lin, Y.-C., & Xu, F.-H. (2013). Decadal warming of coastal China seas and coupling with winter monsoon and currents. *Geophysical Research Letters*, *40*(23), 6288–6292.

Pei, Y. H., Zhang, R. H., & Chen, D. K. (2015). Upper ocean response to tropical cyclone wind forcing: A case study of typhoon Rammasun (2008). *Science China Earth Sciences*, *58*(9), 1623–1632.

Powell, M. D., & Reinhold, T. A. (2007). Tropical cyclone destructive potential by integrated 627 kinetic energy. *Bulletin of the American Meteorological Society*, *88*, 513–526.

Schenkel, B., & Hart, R. E. (2012). An examination of tropical cyclone position and intensity differences within reanalysis datasets. *Journal of Climate*, *25*, 3453–3475. https://doi.org/10.1175/2011JCLI4208.1

Sriver, R., & Huber, M. (2007). Observational evidence for an ocean heat pump induced by tropical cyclones. *Nature*, *447*, 577–580.

Stefanova, L., Misra, V., Chan, S., Griffin, M., O'Brien, J., & Smith, T. (2012). A proxy for high-resolution regional reanalysis for the southeast United States: Assessment of precipitation variability in dynamically downscaled reanalysis. *Climate Dynamics*, *38*, 2449–2466.

Vigh, J. L., Knaff, J. A., & Schubert, W. H. (2012). A climatology of hurricane eye formation. *Monthly Weather Review*, *140*, 1405–1426. https://doi.org/10.1175/MWR-D-11-00108.1

Vukicevic, T., Uhlhorn, E., Reasor, P., & Klotz, B. (2014). A novel multiscale intensity metric for evaluation of tropical cyclone intensity forecasts. *Journal of the Atmospheric Sciences*, *71*(4), 1292–1304.

Yu, J.-Y., & Chiu, P.-G. (2012). Contrasting various metrics for measuring tropical cyclone activity. *Terrestrial, Atmospheric, and Oceanic Sciences*, *23*, 303–316.

Yu, J.-Y., Chou, C., & Chiu, P.-G. (2009). A revised accumulated cyclone energy index. *Geophysical Research Letters*, *36*, L14710. https://doi.org/10.1029/2009GL039254

Zhang, R. –. H., Pei, Y., & Chen, D. (2013). Remote effects of tropical cyclone wind forcing over the western Pacific on the eastern equatorial ocean. *Advances in Atmospheric Sciences*, *30*(6), 1507–1525.

Zheng, C. W., Pan, J., & Li, C. Y. (2016). Global oceanic wind speed trends. *Ocean & Coastal Management*, *129*, 15–24.

Zick, S. E., & Matyas, C. J. (2015). Tropical cyclones in the North American regional reanalysis: An assessment of spatial biases in location, intensity, and structure. *Journal of Geophysical Research: Atmospheres*, *120*(5), 1651–1669.

How to cite this article: Buchanan S, Misra V, Bhardwaj A. Integrated kinetic energy of Atlantic tropical cyclones in a global ocean surface wind analysis. *Int. J. Climatol.* 2018;1–11. https://doi.org/10.1002/joc.5450